RSC Advances

PAPER

View Article Online
View Journal | View Issue

Check for updates

Cite this: *RSC Adv.*, 2017, **7**, 52995

Luminescence properties and energy transfer behavior of colour-tunable white-emitting $Sr_4Al_{14}O_{25}$ phosphors with co-doping of Eu^{2+}, Eu^{3+} and Mn^{4+}

Ziyao Wang, Xifeng Hou,* Yangai Liu,* Zhuang Hui, Zhaohui Huang, Minghao Fang and Xiaowen Wu

Received 20th July 2017
Accepted 3rd November 2017

DOI: 10.1039/c7ra07970b

rsc.li/rsc-advances

Eu^{2+}, Eu^{3+} and Mn^{4+} co-doped $Sr_4Al_{14}O_{25}$ phosphors were synthesized in air by high temperature solid-state reaction. The coexistence of Eu^{2+}, Eu^{3+} and Mn^{4+} in $Sr_4Al_{14}O_{25}$ was detected and verified from X-ray photoelectron spectra (XPS), photoluminescence (PL)/photoluminescence excitation (PLE) spectra and diffuse reflection spectra. The crystal structure, luminescence properties and energy transfer between Eu^{2+} and Mn^{4+} were investigated scientifically. Under ultraviolet excitation, a broad emission band with peak at 496 nm was ascribed to a $4f^65d–4f^7$ transition of Eu^{2+}, and another five narrow emission bands were attributed to 4f–4f transitions of Eu^{3+}. The sharp emission band with peak at 659 nm was generated from the spin-forbidden electronic transition $^2E_g–^4T_2$ of Mn^{4+}. The energy transfer between Eu^{2+} and Mn^{4+} was demonstrated following the nonradiative electric dipole–dipole interaction, and the energy transfer efficiency reached 58.16%. The emission colour of $Sr_4Al_{14}O_{25}$:Eu,Mn^{4+} can be tuned from blue-green (0.2396, 0.3332) to white (0.3465, 0.2906) with increasing concentrations of Mn^{4+}.

Open Access Article. Published on 15 November 2017. Downloaded on 7/22/2024 3:59:27 PM.
This article is licensed under a Creative Commons Attribution 3.0 Unported Licence.

1 Introduction

With the ever-increasing demands of humankind for illumination quality, white light-emitting diodes (WLEDs) are replacing the incandescent and fluorescent lamps gradually and becoming a new generation of solid state lighting sources for buildings and scenery lighting, LCD backlighting, interior lighting, automobiles, agriculture, medicine and aerospace.[1–4] At present, the commercial method to generate white light emission is exciting the yellow-emitting $Y_3Al_5O_{12}:Ce^{3+}$ (YAG:Ce^{3+}) with an InGaN light-emitting diode (LED) chip which emits blue light with the wavelength between 450 nm and 480 nm typically.[5,6] Because of the emission deficiency in the red region, this WLED shows poor colour rendering and appears a simple cool white. Another feasible method is combining blue, green and red phosphors with a near-ultraviolet (n-UV) chip which emits ultraviolet with the wavelength between 380 nm and 420 nm.[7–9] This combination improves the colour rendering performance, but poor chemical stability will be shown as it ages due to the different chemical properties of the three phosphors. Compared with other approaches, studies on the preparation of direct-white-emitting light phosphors have been carried out due to their excellent thermal stability and colour rendering properties.

To the best of our knowledge, aluminate has becoming an important host material because of its excellent thermostability, non-poisonous and competitive price.[10–13] Peng[14] firstly found the coexistence of Eu^{2+} and Eu^{3+} in $Sr_4Al_{14}O_{25}$ prepared in air. Two broad bands peaking at 400 nm and 490 nm attributed to the 4f–5d transition of Eu^{2+}, and line emissions in the region of 550–700 nm belong to the f–f transitions of Eu^{3+}. Xu[15] reported the non-RE activated $Sr_4Al_{14}O_{25}:Mn^{4+}$ phosphor prepared by solid-state method in air. The Al^{3+} ions in the [AlO_6] octahedral sites of $Sr_4Al_{14}O_{25}$ were substituted by Mn^{4+} ions in the crystal lattice, and the emission spectrum measurement excited by 365 nm showed that the sharp emission peak at 651 nm was ascribed to the $^2E–^4A_2$ transition of Mn^{4+} ion, and a broad band at 662 nm was attributed to the phonon sideband transition. Based on the above experimental results, the authors believe that there should be an energy transfer between Eu^{2+} and Mn^{4+} in $Sr_4Al_{14}O_{25}$. Meanwhile, there has been no one, by far, reporting its luminescence properties and potential applications. The previous studies provide the access to obtain direct white emission for WLED by the coexistence of Eu^{2+}, Eu^{3+} and Mn^{4+} in $Sr_4Al_{14}O_{25}$.

In our work, a series of $Sr_4Al_{14}O_{25}:x$Eu,Mn^{4+} phosphors were synthesized in air through the high temperature solid-state

Beijing Key Laboratory of Materials Utilization of Nonmetallic Minerals and Solid Wastes, National Laboratory of Mineral Materials, School of Materials Science and Technology, China University of Geosciences, Beijing 100083, P. R. China. E-mail: liuyang@cugb.edu.cn; houxifeng3204114@126.com; Fax: +86-10-82322186; Tel: +86-10-82322186

Open Access Article. Published on 15 November 2017. Downloaded on 7/22/2024 3:59:27 PM.
This article is licensed under a Creative Commons Attribution 3.0 Unported Licence.

reaction. The coexistence of Eu^{2+}, Eu^{3+} and Mn^{4+} was revealed by X-ray photoelectron spectroscopy (XPS), diffuse reflection spectra and photoluminescence (PL) spectra. The influences of Mn^{4+} on the luminescence properties were discussed in detail, and the fluorescence lifetime, energy transfer between Eu^{2+} and Mn^{4+} and applications in WLED were studied respectively.

2 Experimental

Series of Eu^{3+} ions single-doped $Sr_4Al_{14}O_{25}$:xEu (x = 0.005, 0.01, 0.02, 0.04, 0.06, 0.08) and co-doped $Sr_4Al_{14}O_{25}$:0.01Eu,$y$$Mn^{4+}$ (y = 0.0002, 0.0005, 0.001, 0.002, 0.003, 0.005, 0.01, 0.02) were synthesized by conventional solid-state reaction in air with $SrCO_3$(A.R.), $Al(OH)_3$(A.R.), $MnCO_3$(A.R.), H_3BO_3(A.R.) and Eu_2O_3(4N). The stoichiometric amount of raw materials were well homogenized in an agate mortar, and the H_3BO_3 was added as a flux. All samples were pre-sintered in alumina crucibles in air at 700 °C for 2 h, and further heat-treated at 1400 °C for 5 h with sufficient grindings in the processes.

The phase purity of synthesized phosphors were checked by X-ray diffraction (XRD) with a D8 Advance diffractometer with Cu Kα radiation (λ = 1.5406 Å) by the step of 4° min^{-1} at room temperature. The X-ray photoelectron spectroscopy (XPS) was obtained on an ESCALAB 250xi (ThermoFisher, England) electron spectrometer. The emission and excitation spectra were analyzed on a Hitachi F-4600 fluorescence spectrophotometer with a 400 nm cut-off filter. The diffuse reflection spectra were detected by a Shimadzu UV-3600 UV-vis-NIR spectrophotometer attached with an integral sphere. The photoluminescence decay curves were recorded on a Horiba JOBIN YVON FL3-21 spectrofluorometer.

3 Results and discussion

Fig. 1 shows the XRD patterns of $Sr_4Al_{14}O_{25}$:xEu (x = 0, 0.005, 0.01, 0.02, 0.04, 0.06) and $Sr_4Al_{14}O_{25}$:0.01Eu,$y$$Mn^{4+}$ (y = 0.0002, 0.0005, 0.001, 0.002, 0.003, 0.005, 0.01) synthesized at 1400 °C for 5 h in air. The reference pattern of the standard JCPDS Card no. 52-1876 for $Sr_4Al_{14}O_{25}$ was also listed in Fig. 1 as a reference. It is observed that the samples synthesized in various conditions are all in pure $Sr_4Al_{14}O_{25}$ phase, and the change of doping of Eu^{3+} and Mn^{4+} ions would not impact the host structure.

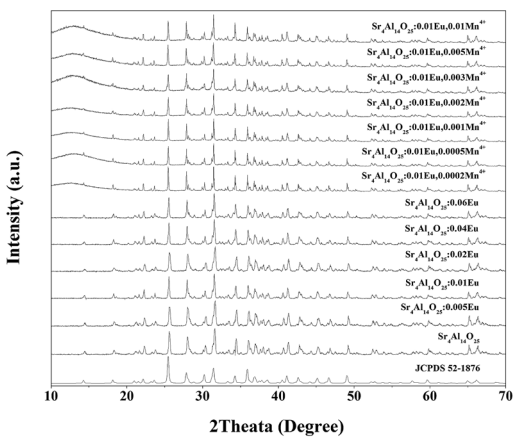

Fig. 1 XRD patterns of $Sr_4Al_{14}O_{25}$:xEu (x = 0, 0.005, 0.01, 0.02, 0.04, 0.06) and $Sr_4Al_{14}O_{25}$:0.01Eu,$y$$Mn^{4+}$ (y = 0.0002, 0.0005, 0.001, 0.002, 0.003, 0.005, 0.01) synthesized at different temperatures, and the standard pattern JCPDS 52-1876.

It has been found that the Mn^{4+} ion is more likely to achieve stability once it is accommodated and stabilized in an octahedral site. Usually, there will be strong absorption and emission spanning from 250 nm to 500 nm and 630 nm to 735 nm respectively when Mn^{4+} substitutes an octahedral site.[16,17] The fragments of $Sr_4Al_{14}O_{25}$ unit cell are exhibited in Fig. 2. $Sr_4Al_{14}O_{25}$ is orthorhombic structure with space group *Pmma*. The structure contains two Sr sites and six Al sites. Sr(1) and Sr(2) are both coordinated by ten oxygen atoms. Al(1), Al(2) and Al(3) form tetrahedrons with four coordinations, while Al(4), Al(5) and Al(6) are six-coordinated that form rigid octahedrons.[18] Because the radius difference between Eu^{2+} and Sr^{2+} ions is much smaller than that of Eu^{2+} and Al^{3+}, and the ionic size of Mn^{4+} is much smaller than that of Sr^{2+} but close to Al^{3+}, it is reasonable to consider the Eu^{2+} ions are substituted in Sr^{2+} sites, while Mn^{4+} ions tend to occupy the octahedral sites of Al^{3+}.

Fig. 3 shows the observed (black squares), calculated (red lines), and difference (bottom) XRD profiles for the Rietveld refinement of $Sr_{3.96}Al_{13.9972}O_{25}$:0.04$Eu^{2+}$,0.0028$Mn^{2+}$ with λ = 1.5406 Å by TOPAS program. Almost all peaks can be indexed by hexagonal cell with parameters close to $Sr_4Al_{14}O_{25}$, herein the structural parameters of $Sr_4Al_{14}O_{25}$ are used as initial parameters in the Rietveld analysis. The final refinement is stable and convergent well with low residual factors R_{exp} = 6.281%, R_{wp} = 17.843%, R_p = 13.770% and χ^2 = 2.841, indicating the single phase with no unidentified diffraction peaks from impurity.

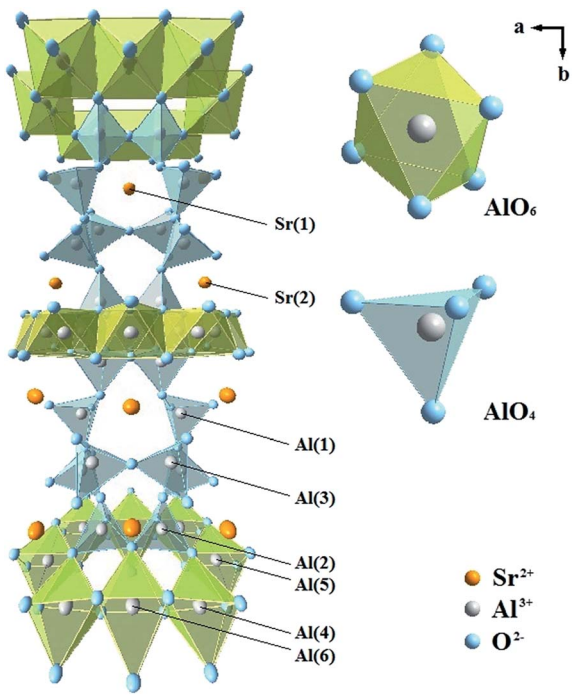

Fig. 2 The crystal structures of $Sr_4Al_{14}O_{25}$.

This journal is © The Royal Society of Chemistry 2017

Open Access Article. Published on 15 November 2017. Downloaded on 7/22/2024 3:59:27 PM.
This article is licensed under a Creative Commons Attribution 3.0 Unported Licence.

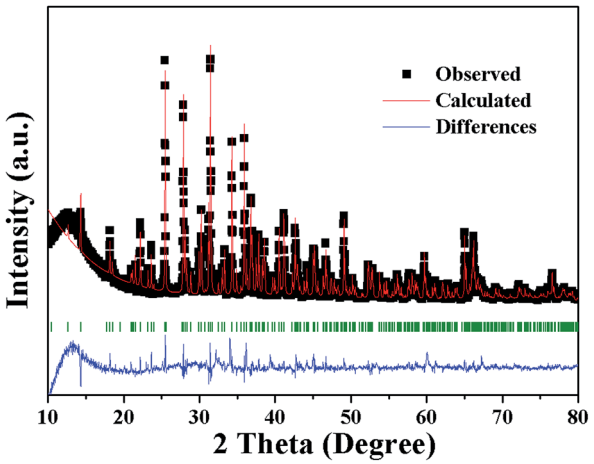

Fig. 3 Power XRD pattern of $Sr_{3.96}Al_{13.9972}O_{25}$:0.04$Eu^{2+}$,0.0028$Mn^{2+}$ with corresponding Rietveld refinement (red) and residuals (blue).

The final refined crystallographic data are listed in Table 1. The cell parameters are determined to be $a = 24.7177$ Å, $b = 8.4810$ Å, $c = 4.8847$ Å and $V = 1026.22$ Å^3. The crystallographic site coordinates, occupancy factors, and equivalent isotropic displacement parameters are summarized in Table 2.

To examine the valence state of europium and manganese in $Sr_4Al_{14}O_{25}$, the XPS spectra of $Sr_4Al_{14}O_{25}$:xEu (x = 0.01, 0.02, 0.06) and $Sr_4Al_{14}O_{25}$:0.01Eu,$y$$Mn^{4+}$ (y = 0.005, 0.01, 0.02) is recorded in Fig. 4(a) and (b). It is evident from Fig. 4(a) that the broad bands peaking at 1136.5 eV ascribed to Eu^{3+} $3d_{5/2}$ are observed, and the bands peaking at 1127.5 eV consistent with Eu^{2+} $3d_{5/2}$ emerge gradually with the increasing doping of Eu^{3+} ions.[19] The peak intensities of Mn^{4+} $2p_{3/2}$ and $2p_{1/2}$ at 642.5 eV and 654.5 eV, as shown in Fig. 4(b), increase with the increasing content of Mn^{2+} ions, and no Mn^{2+} peaks are observed as the value of y varies. We can deeply confirm that there is an coexistence of Eu^{2+}, Eu^{3+} and Mn^{4+} in $Sr_4Al_{14}O_{25}$ phosphors.

Fig. 5 shows the excitation and emission spectra of $Sr_4Al_{14}O_{25}$:Eu. We doped the Eu ions originally into the host in the form of Eu_2O_3, and we found that the trivalent and bivalent Eu ions co-existed in $Sr_4Al_{14}O_{25}$:Eu prepared in air at 1400 °C for 5 h. Under 496 nm monitoring, as shown in Fig. 5(a), the broad excitation band from 250 nm to 450 nm with maximum at 362 nm originates from the f–d transition of Eu^{2+}.[20] The other excitation spectra monitored at 619 nm consists of the broad bands from 200 nm to 350 nm, which is generated from the charge-transfer band (CTB) between Eu^{3+} and O^{2-} with the peak at 261 nm, and the series of narrow bands from 350 nm to 550 nm form from the f–f transition of Eu^{3+} within its $4f^6$ configuration.[21] The PL spectra with different excitation factors are demonstrated in Fig. 5(b). The characteristic peaks of Eu^{2+} and Eu^{3+} are both observed in emission spectra with the change of excitation wavelength. The band emission peaking at 469 nm stems from $4f^65d$–$4f^7$ transition of Eu^{2+}, and the other five typical line emissions peaking at 596 nm, 620 nm, 652 nm, 688 nm and 707 nm are attributed to 4f–4f transition of $^5d_0$–^7f_J ($J = 1, 2, 3, 4$) of Eu^{3+}.[22,23] The strongest emission generated from the transition of $^5d_0$–$^7f_2$ of Eu^{3+} belongs to the electric dipole transition, which reflects that the electric dipole transition is the dominant factor in the luminescence process of Eu^{3+}.[24]

The PL spectra of $Sr_4Al_{14}O_{25}$:xEu (x = 0.005, 0.01, 0.02, 0.04, 0.06, 0.08) prepared at 1400 °C for 5 h and the dependence of the relative emission intensities of Eu^{2+} (496 nm) and Eu^{3+} (594 nm) in the $Sr_4Al_{14}O_{25}$ phosphors are labelled in Fig. 6. All investigated phosphors were monitored at an excitation wavelength of 325 nm. It is found that the PL intensities of red and blue emissions change obviously with the concentration variation of the Eu dopant. The emissions of Eu^{2+} and Eu^{3+} enhance with the increase of Eu^{3+} ions concentration, and the former reaches the maximum at 1 mol% due to the concentration

Table 1 Main parameters of processing and refinement of the $Sr_{3.96}Al_{13.9972}O_{25}$:0.04$Eu^{2+}$,0.0028$Mn^{2+}$ sample

Sp.Gr.	*Pmma*
a, Å	24.7177 (8)
B, Å	8.4810 (3)
c, Å	4.8847 (2)
V, Å^3	1026.22 (6)
2θ-interval, °	10–80
No. of reflections	313
No. of refined parameters	47
R_{wp}, %	17.843
R_p, %	13.770
R_{exp}, %	6.281
χ^2	2.841
R_B, %	4.593

Table 2 Fractional atomic coordinates and isotropic displacement parameters (Å^2) of $Sr_{3.96}Al_{13.9972}O_{25}$:0.04$Eu^{2+}$,0.0028$Mn^{2+}$ sample

$Sr_{3.96}Al_{13.9972}O_{25}$:0.04$Eu^{2+}$,0.0028$Mn^{2+}$

	x	y	z	B_{iso}	*Occ.*
Sr1	0.1387	1/2	0.0355	2.98	0.99
Eu1	0.1387	1/2	0.0355	2.98	0.01
Sr2	0.1204	0	0.1143	1.16	0.99
Eu2	0.1204	0	0.1143	1.16	0.01
Al1	0.1851	0.1956	0.6284	3.68	0.9998
Mn1	0.1851	0.1956	0.6284	3.68	0.0002
Al2	0.0677	0.3178	0.5066	0.35	0.9998
Mn2	0.0677	0.3178	0.5066	0.35	0.0002
Al3	1/4	0.2451	0.4131	1.38	0.9998
Mn3	1/4	0.2451	0.4131	1.38	0.0002
Al4	0	0.1671	0	2.21	0.9998
Mn4	0	0.1671	0	2.21	0.0002
Al5	0	0	1/2	2.98	0.9998
Mn5	0	0	1/2	2.98	0.0002
Al6	0	1/2	0	4.29	0.9998
Mn6	0	1/2	0	4.29	0.0002
O1	0.0462	0.1867	0.3054	1.10	1
O2	0.1359	0.3187	0.5089	1.10	1
O3	0.1904	0.2482	0.9582	1.10	1
O4	1/4	0.2957	0.1281	1.10	1
O5	0.0340	0	0.8224	1.10	1
O6	0.0527	1/2	0.3277	1.10	1
O7	0.1582	0	0.5656	1.10	1
O8	0.0442	0.3234	0.8311	1.10	1
O9	1/4	1/2	0.0580	1.10	1

Open Access Article. Published on 15 November 2017. Downloaded on 7/22/2024 3:59:27 PM.
This article is licensed under a Creative Commons Attribution 3.0 Unported Licence.

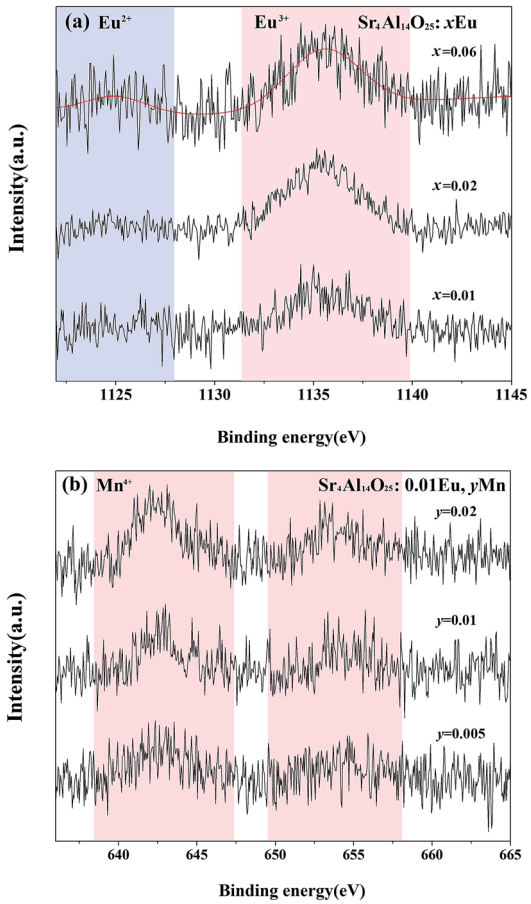

Fig. 4 High-resolution Eu 3d XPS spectra of $Sr_4Al_{14}O_{25}$:xEu ($x = 0.01$, 0.02, 0.06) (a) and Mn 2p XPS spectra of $Sr_4Al_{14}O_{25}$:0.01Eu,yMn ($y = 0.005$, 0.01, 0.02) (b).

quenching.[25] This observation indicates that the increasing doping of Eu^{3+} ions spawn the V''_{Sr} and electrons which can combine with Eu^{3+} ions and promotes the self-reduction reaction in some extent. The self-reduction process can be presented in the following equations:[26]

$$3Sr^{2+} + 2Eu^{3+} \rightarrow V''_{Sr} + 2Eu^{\bullet}_{Sr} \quad (1)$$

$$V''_{Sr} \rightarrow V_{Sr}{}^{x} + 2e \quad (2)$$

$$2Eu^{\bullet}_{Sr} + 2e \rightarrow 2Eu_{Sr}{}^{x} \quad (3)$$

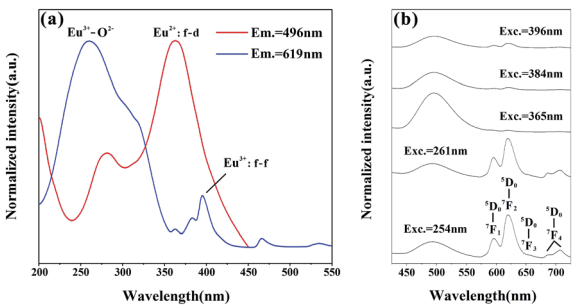

Fig. 5 PLE spectra of Eu^{3+} (619 nm) and Eu^{2+} (496 nm) of $Sr_4Al_{14}O_{25}$:0.01Eu (a) and PL spectra with different excitations (b).

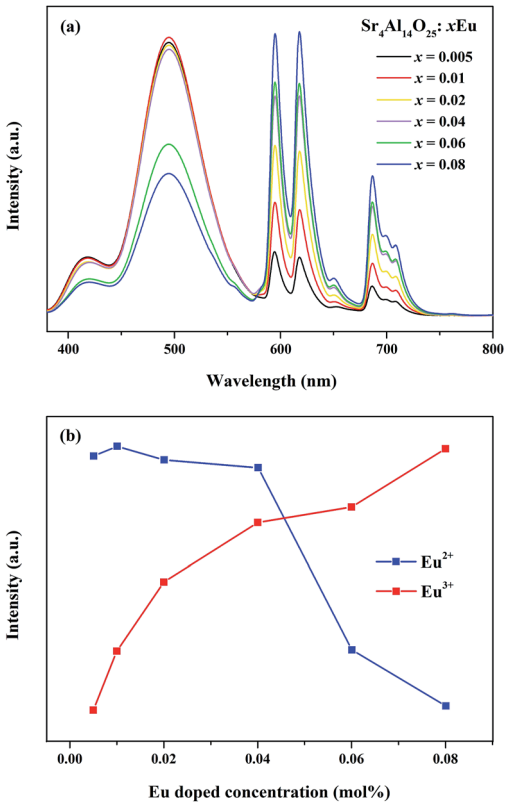

Fig. 6 PL spectra of $Sr_4Al_{14}O_{25}$:xEu ($x = 0.005$, 0.01, 0.02, 0.04, 0.06, 0.08) under ultraviolet excitation (325 nm) (a) and dependence of relative emission intensity of Eu^{2+} (496 nm) and Eu^{3+} (619 nm) in $Sr_4Al_{14}O_{25}$ phosphors as a function of Eu^{3+} doped concentration (b).

As the Mn^{2+} is singly doped in $Sr_4Al_{14}O_{25}$ host, the PL and PLE spectra of synthesized phosphor ($Sr_4Al_{14}O_{25}$:0.002Mn^{4+}) are shown in the Fig. 7. It contains two excitation bands from 250 nm to 550 nm, which are due to the spin-allowed electronic transition $^4A_2$–$^4T_1$ and $^4A_2$–$^4T_2$ of Mn^{4+}.[27] The optimal excitation wavelength of $Sr_4Al_{14}O_{25}$:0.002Mn^{4+} is 325 nm, and the half-band width is approximately 85 nm, much wider than the emission band of UV LED chips. It is indicated that the excitation wavelength at 325 nm can be an alternative for the typical commercial chips in the future market. The sharp emission

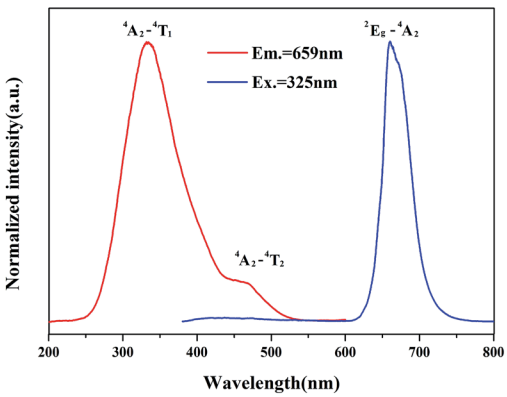

Fig. 7 The spectral pattern of $Sr_4Al_{14}O_{25}$:0.002Mn^{4+}.

This journal is © The Royal Society of Chemistry 2017

Open Access Article. Published on 15 November 2017. Downloaded on 7/22/2024 3:59:27 PM.
This article is licensed under a Creative Commons Attribution 3.0 Unported Licence.

band peaking at 659 nm generates from the spin-forbidden electronic transition ^2E_g–$^4T_2$ of Mn^{4+}.[28]

As revealed in Fig. 8, series of phosphors with varied Eu^{3+} and Mn^{4+} concentrations are synthesized and their PL spectra are recorded upon excitation of 325 nm for the investigation of the energy transfer(ET) between Eu^{2+} and Mn^{4+}. We can see that the intensities of the Eu^{2+} and Eu^{3+} emissions are found to decrease monotonically with increasing Mn^{4+} content due to the conspicuous energy transfer between Eu^{2+} and Mn^{4+}. The simplified diagram of the energy transfer process from Eu^{2+} to Mn^{4+} in $Sr_4Al_{14}O_{25}$ phosphors is illustrated in Fig. 9. As indicated in this diagram, the relationship of energy transfer between Eu^{2+} and Mn^{4+} ions can be attributed to the similar energy level values between the excited 5d state of Eu^{2+} and the $^4T_{1g}$ levels of Mn^{4+} ions.[29]

Meanwhile, the PL intensity of the Mn^{4+} increases with the doping of Mn^{4+} ions, and comes to a maximum value at y = 0.001. Then the concentration quenching leads to the weakening of PL intensity. The synthesized phosphors can be tuned expediently from blue-green to white by the co-existence of Eu^{2+}, Eu^{3+} and Mn^{4+}. To observe the characteristic of change in colour after doping Mn^{4+} more visually, as shown in Table 3 and Fig. 10, the Commission Internationale de l'Eclairage (CIE) chromaticity coordinates, correlated colour temperature (CCT) and CIE chromaticity diagram of $Sr_4Al_{14}O_{25}$:0.01Eu,$y$$Mn^{4+}$

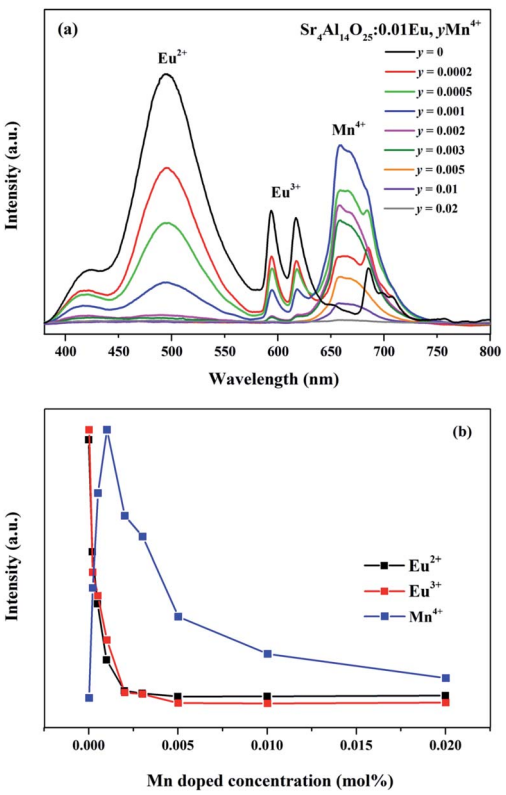

Fig. 8 PL spectra of $Sr_4Al_{14}O_{25}$:0.01Eu,$y$$Mn^{4+}$ (y = 0, 0.0002, 0.0005, 0.001, 0.002, 0.003, 0.005, 0.01, 0.02) under ultraviolet excitation (325 nm) (a) and dependence of relative emission intensity of Eu^{2+} (496 nm), Eu^{3+} (619 nm) and Mn^{4+} (659 nm) in $Sr_4Al_{14}O_{25}$ phosphors as a function of Mn^{4+} doped concentration (b).

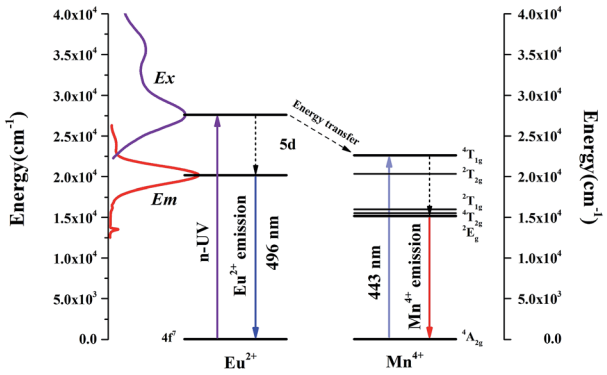

Fig. 9 The energy level structure of Eu^{2+} and Mn^{4+} and the energy transfer mechanism among them.

Table 3 The CIE chromaticity coordinates (x, y) and correlated colour temperature (CCT) of $Sr_4Al_{14}O_{25}$:0.01Eu,$y$$Mn^{4+}$ (y = 0, 0.0002, 0.0005, 0.001)

Sample no.	Composition (y)	CIE coordinates (x, y)	CCT (K)
1(a)	0	(0.2396, 0.3332)	11 489
2(b)	0.0002	(0.2723, 0.3191)	9380
3(c)	0.0005	(0.3266, 0.3040)	5798
4(d)	0.001	(0.3465, 0.2906)	4554

(y = 0, 0.0002, 0.0005, 0.001) phosphors are calculated and plotted respectively. As summarized in Table 2, the series of chromaticity coordinates of the $Sr_4Al_{14}O_{25}$:0.01Eu,$y$$Mn^{4+}$ are calculated from the corresponding datum of emission spectra. The phosphors can be regulated from blue-green (0.2396, 0.3332) to white (0.3465, 0.2906) with the increasing concentration of Mn^{4+}, corresponding to the correlated colour temperature from 11 489 K to 4554 K as listed in Table 3.

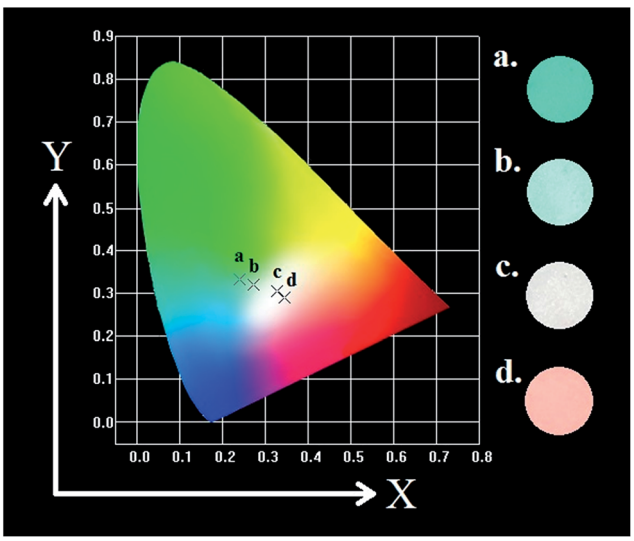

Fig. 10 CIE chromaticity diagram of $Sr_4Al_{14}O_{25}$:0.01Eu,$y$$Mn^{4+}$ (y = 0, 0.0002, 0.0005, 0.001) under 325 nm excitation and digital images in UV box.

Open Access Article. Published on 15 November 2017. Downloaded on 7/22/2024 3:59:27 PM.
This article is licensed under a Creative Commons Attribution 3.0 Unported Licence.

To further verify the existence of energy transfer between Eu^{2+} and Mn^{4+} in $Sr_4Al_{14}O_{25}$:0.01Eu,yMn^{4+} ($y = 0$, 0.0005, 0.001, 0.002, 0.003, 0.005, 0.01, 0.02), we investigated the luminescence decay curves of Eu^{2+} 496 nm emission and the corresponding lifetimes of Eu^{2+} with the doping of Mn^{4+}. Additionally, the energy transfer efficiency is also listed next to the lifetimes in Fig. 11(a). All the decay curves can be well fitted ground on the following non-exponential equation:[30,31]

$$\tau = \frac{\int_0^\infty I(t)t\mathrm{d}t}{I(t)\mathrm{d}t} \quad (4)$$

where $I(t)$ stands for the PL intensities at time t. The effective decay lifetimes monitored at 496 nm of Eu^{2+} are calculated to be 1478.69, 1242.81, 888.22, 794.80, 720.49, 652.35, 643.00 and 618.70 ns for $y = 0$, 0.0005, 0.001, 0.002, 0.003, 0.005, 0.01, 0.02, respectively. The lifetimes of Eu^{2+} emission are monotonically decreasing with the doping of Mn^{4+}, which indicates that the energy transfer between Eu^{2+} and Mn^{4+} ions occurs in the $Sr_4Al_{14}O_{25}$ host, and the estimate the Eu^{2+}–Mn^{4+} ET probability (P_{Eu-Mn}) can be fitted to the following equation:[32,33]

$$P_{Eu-Mn} = \frac{1}{\tau_y} - \frac{1}{\tau_0} \quad (5)$$

where τ_y and τ_0 stand for the corresponding lifetimes of Eu^{2+} ions with and without Mn^{4+} ions doping for the constant sensitizer concentration. The values of the estimated P_{Eu-Mn} are plotted in Fig. 11(b). The consecutive increasing of the ET probabilities with the various Mn^{4+} content manifests an enhanced ET process between Eu^{2+} and Mn^{4+} because of the decrease in the average distance between the ions.[34] Furthermore, the energy transfer efficiency η from a donor Eu^{2+} to acceptor Mn^{4+} would be estimated according to the expression as follows:[35]

$$\eta = 1 - \frac{\tau_S}{\tau_{S_0}} \quad (6)$$

where η stands for the energy transfer efficiency. τ_s and τ_{s_0} mean the lifetimes of Eu^{2+} with and without the doping of Mn^{4+} ions. As shown in the Fig. 11(a), the energy transfer efficiency decreases constantly from 15.95% to 58.16% with the increasing concentration of Mn^{4+}. The result is ascribed to the shortening distance between the Eu^{2+} ions and Mn^{4+} ions.

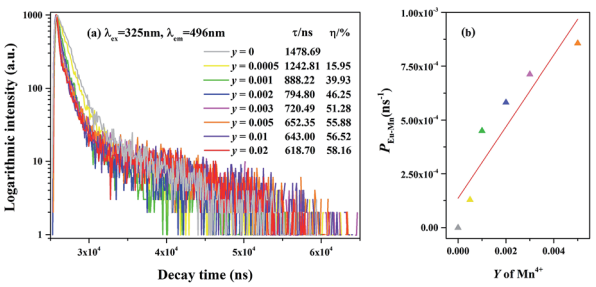

Fig. 11 Decay curves, lifetime and energy transfer efficiency (η) of $Sr_4Al_{14}O_{25}$:0.01Eu,yMn^{4+} ($y = 0$, 0.0005, 0.001, 0.002, 0.003, 0.005, 0.01, 0.02) under excitation of 325 nm (a). Energy transfer probability (P_{Eu-Mn}) as a function of Mn^{4+} doped concentration.

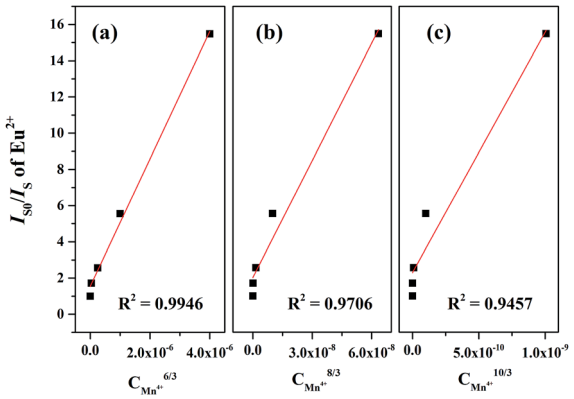

Fig. 12 Dependence of I_{s_0}/I_s of Eu^{2+} on $C_{Mn}^{6/3}$, $C_{Mn}^{8/3}$ and $C_{Mn}^{10/3}$.

Generally, the energy transfer mechanism between the sensitizer (Eu^{2+}) to activator (Mn^{4+}) ions and the relation can be revealed by the Dexter's energy transfer theory:[36–38]

$$\frac{I_{S_0}}{I_S} \propto C^{n/3} \quad (7)$$

in which I_{s_0} and I_s mean the PL intensities of Eu^{2+} with and without activator Mn^{4+} ions, separately. C stands for the doping content of Mn^{4+} ions, and the dipole–dipole, dipole–quadrupole, and quadrupole–quadrupole interactions correspond to $n = 6$, 8, and 10, respectively. The fitting curves of I_{s_0}/I_s *versus* $C^{n/3}$ are shown in Fig. 12(a–c), which reveal a linearity only when $n = 6$, demonstrating that the energy transfer mechanism from Eu^{2+} to Mn^{4+} in the $Sr_4Al_{14}O_{25}$ host follows a nonradiative electric dipole–dipole interaction.

Fig. 13 presents the diffuse reflection spectra of $Sr_4Al_{14}O_{25}$, $Sr_4Al_{14}O_{25}$:0.01Eu and $Sr_4Al_{14}O_{25}$:0.01Eu,0.003Mn^{4+}. It is observed that the energy absorption of $Sr_4Al_{14}O_{25}$ host occurs in ultraviolet region, and the band gap is estimated to be 3.701 eV based on the fitting line of the absorption edge.[39,40] A strong energy absorption band can be seen obviously in the 200–350 nm region from the host material. With the doping of Eu^{3+} ions, an obvious absorption appears around 200–300 nm in the near-UV region as a result of the 4f–5d transition of Eu^{2+},

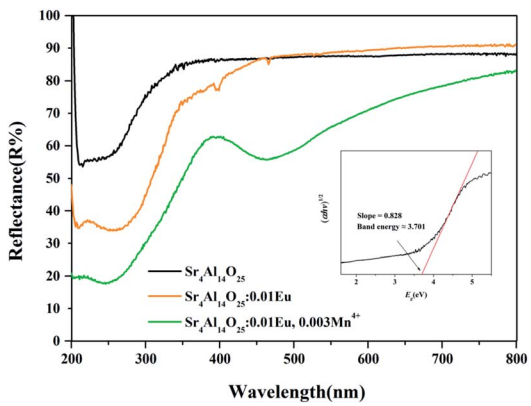

Fig. 13 Diffuse reflectance spectra of $Sr_4Al_{14}O_{25}$, $Sr_4Al_{14}O_{25}$:0.01Eu and $Sr_4Al_{14}O_{25}$:0.01Eu,0.003Mn^{4+}.

This journal is © The Royal Society of Chemistry 2017

Open Access Article. Published on 15 November 2017. Downloaded on 7/22/2024 3:59:27 PM.
This article is licensed under a Creative Commons Attribution 3.0 Unported Licence.

and the relatively weak absorption peaking at 391 nm results from the f–f transition of Eu^{3+}, which is in accordance with the excitation spectra of Eu^{2+} and Eu^{3+}. When the Mn^{4+} doped into the host, it exhibits an obvious absorption from 390 nm to 550 nm assigned to the spin-forbidden electronic transition of the Mn^{4+} ions. Above results indicates the potential of $Sr_4Al_{14}O_{25}$:Eu,Mn^{4+} for solid-state lighting.

4 Conclusion

Series of colour-tunable direct-white-emitting phosphors $Sr_4Al_{14}O_{25}$:Eu,Mn^{4+} were synthesized in air by conventional high temperature solid state reactions. The coexistence of Eu^{2+}, Eu^{3+} and Mn^{4+} was proved, and the self-reduction process of Eu^{3+} was discussed. The luminescence properties were investigated, and three groups of emissions in $Sr_4Al_{14}O_{25}$ ascribed to Eu^{2+}, Eu^{3+} and Mn^{4+} were observed under ultraviolet excitation. The energy transfer between Eu^{2+} and Mn^{4+} originated from a nonradiative electric dipole–dipole interaction, and the energy transfer efficiency could reach 58.16%. The emission colour of $Sr_4Al_{14}O_{25}$:0.01Eu,$y$$Mn^{4+}$ (y = 0, 0.0002, 0.0005, 0.001) could be modulated from blue-green (0.2396, 0.3332) to white (0.3465, 0.2906), corresponding to the colour temperature from 11 489 K to 4554 K with the increasing concentration of Mn^{4+}. These results manifest that the prepared $Sr_4Al_{14}O_{25}$:Eu,Mn^{4+} phosphor can be regarded as a potential approach to obtain colour-tunable direct-white emissions through adjusting the content of Mn^{4+}.

Conflicts of interest

There are no conflicts to declare.

Acknowledgements

We thank the National Natural Science Foundation of China (Grant No. 51472223) and the Fundamental Research Funds for Central Universities (Grant No. 2652015090).

Notes and references

1 B. Ma, Q. F. Guo, M. S. Molokeev, *et al.*, *Ceram. Int.*, 2016, **42**, 5995–5999.
2 R. Y. Mi, C. L. Zhao and Z. G. Xia, *J. Am. Ceram. Soc.*, 2014, **97**, 1802–1808.
3 D. L. Geng, G. G. Li, M. M. Shang, *et al.*, *J. Mater. Chem.*, 2012, **22**, 14262–14271.
4 Z. Y. Wang, J. Chen, Y. G. Liu, *et al.*, *J. Adv. Ceram.*, 2017, **6**, 81–89.
5 Y. T. Lin, Z. R. Niu, Y. Han, *et al.*, *J. Alloys Compd.*, 2017, **690**, 267–273.
6 Y. F. Xia, J. Chen, Y. G. Liu, *et al.*, *Mater. Express*, 2016, **6**, 37–44.
7 M. Lee and W. Jung, *Ceram. Int.*, 2016, **42**, 3113–3120.
8 T. Arakawa and N. Nagata, *J. Alloys Compd.*, 2006, **408–412**, 864–866.
9 A. D. Deshmukh, S. J. Dhoble and N. S. Dhoble, *Adv. Mater. Lett.*, 2011, **2**, 38–42.
10 L. J. Xiao, M. R. He, Y. W. Tian, *et al.*, *J. Nanosci. Nanotechnol.*, 2010, **10**, 2131–2134.
11 M. Y. Peng, J. R. Qiu, L. Y. Yang, *et al.*, *Opt. Mater.*, 2004, **27**, 591–595.
12 M. Y. Peng and G. Hong, *J. Lumin.*, 2007, **127**, 735–740.
13 M. Rezende, M. Valerio and R. Jackson, *Mater. Res. Bull.*, 2014, **61**, 348–351.
14 M. Y. Peng, Z. W. Pei, G. Hong, *et al.*, *Chem. Phys. Lett.*, 2003, **371**, 1–6.
15 Y. D. Xu, D. Wang, L. Wang, *et al.*, *J. Alloys Compd.*, 2013, **550**, 226–230.
16 M. Y. Peng, Z. W. Pei, G. Hong, *et al.*, *J. Mater. Chem.*, 2003, **13**, 1202–1205.
17 M. Y. Peng, X. W. Yin, P. Tanner, *et al.*, *Chem. Mater.*, 2015, **27**, 2938–2945.
18 Y. H. Lin, Z. L. Tang, Z. T. Zhang, *et al.*, *Appl. Phys. Lett.*, 2002, **81**, 996–998.
19 J. Chen, Y. G. Liu, H. K. Liu, *et al.*, *Opt. Mater.*, 2015, **42**, 80–86.
20 Z. G. Xia, R. S. Liu, K. W. Huang, *et al.*, *J. Mater. Chem.*, 2012, **22**, 15183–15189.
21 R. Y. Mi, J. Chen, Y. G. Liu, *et al.*, *RSC Adv.*, 2016, **6**, 28887–28894.
22 H. K. Liu, Q. F. Guo, L. B. Liao, *et al.*, *Opt. Commun.*, 2013, **309**, 64–67.
23 Z. G. Xia, J. Zhou and Z. Y. Mao, *J. Mater. Chem. C*, 2013, **1**, 5917–5924.
24 J. Chen, Y. G. Liu, L. F. Mei, *et al.*, *J. Mater. Chem. C*, 2015, **3**, 3451–3455.
25 H. K. Liu, Y. Y. Zhang, L. B. Liao, *et al.*, *J. Lumin.*, 2014, **156**, 49–54.
26 Q. H. Zeng, Z. W. Pei, S. B. Wang, *et al.*, *J. Alloys Compd.*, 1998, **275–277**, 238–241.
27 Y. Zhydachevskii, D. Galanciak, S. Kobyakov, *et al.*, *J. Phys.: Condens. Matter*, 2006, **18**, 11385.
28 S. Adachi and T. Takahashi, *J. Appl. Phys.*, 2008, **104**, 317.
29 S. Adachi and T. Takahashi, *J. Appl. Phys.*, 2009, **106**, 339.
30 R. J. Xie, N. Hirosaki, N. Kimura, *et al.*, *Appl. Phys. Lett.*, 2007, **90**, 191101.
31 Y. Y. Zhang, Z. G. Xia, H. K. Liu, *et al.*, *Chem. Phys. Lett.*, 2014, **593**, 189.
32 M. Xie, T. Ye, Y. Huang, *et al.*, *ChemInform*, 2011, 42.
33 D. Wen, J. Feng, J. Li, *et al.*, *J. Mater. Chem. C*, 2015, **3**, 2107–2114.
34 J. Chen, C. H. Li, Z. Hui, *et al.*, *Inorg. Chem.*, 2017, **56**, 1144–1151.
35 W. J. Yang, L. Y. Luo, T. M. Chen, *et al.*, *Chem. Mater.*, 2005, **17**, 3883–3888.
36 D. L. Dexter and J. H. Schulman, *J. Chem. Phys.*, 1954, **22**, 1063–1070.
37 S. P. Lee, C. H. Huang and T. M. Chen, *J. Mater. Chem. C*, 2014, **2**, 8925–8931.
38 D. Y. Wang, C. H. Huang, B. M. Cheng, *et al.*, *RSC Adv.*, 2014, **4**, 28632–28635.
39 Y. F. Xia, Y. G. Liu, Z. H. Huang, *et al.*, *J. Mater. Chem. C*, 2016, **4**, 4675–4683.
40 C. Zeng, H. W. Huang, Y. M. Hu, *et al.*, *RSC Adv.*, 2015, **5**, 68099–68108.